Experimental Thermal and Fluid Science 176 (2026) 111760

Contents lists available at ScienceDirect

Experimental Thermal and Fluid Science

journal homepage: www.elsevier.com/locate/etfs

In-tube condensation of a zeotropic mixture: Impact of uncertainties in the experimental design and in mixture properties on heat transfer coefficients

Clemens Berger [a,*], Leonard Schnelting [b,c], Gabriele Raabe [b], Matthias Welzl [a], Florian Heberle [a], Dieter Brüggemann [a]

[a] Chair of Engineering Thermodynamics and Transport Processes, Center of Energy Technology, University of Bayreuth, Universitätsstraße 30, 95440 Bayreuth, Germany

[b] Institute of Thermodynamics, Technische Universität Braunschweig, Hans-Sommer-Straße 5, 38106 Braunschweig, Germany

[c] Institute for Acoustics and Dynamics, Technische Universität Braunschweig, Langer Kamp 19, 38106 Braunschweig, Germany

ARTICLE INFO

Keywords:
Stratified flow condensation
R134a
R1233zd(E)
Interaction parameters
Helmholtz Equation of State
Molecular simulations

ABSTRACT

Zeotropic mixtures are of growing interest for thermodynamic cycle applications due to an efficiency improvement by glide matching. One key factor in the development of mixture applications is research on heat transfer characteristics as generally lower heat transfer coefficients in comparison to pure fluids could counteract higher efficiencies. Due to the complex fluid behaviour of mixtures simplifications are applied in the evaluation of measurements, affecting the resulting heat transfer coefficients. This study investigates the condensation heat transfer for a zeotropic mixture R134a/R1233zd(E) with focus on the impact of different methodologies for the evaluation of measurement data. The main aspect is the fluid temperature definition by either measurement or calculation, which has a great influence on the determination of heat transfer coefficients. Additionally, the impact of available mixture properties is investigated by molecular simulations and fitting of binary interaction parameters. A comparison with the standard approximated interaction parameters is made with respect to composition and state point calculations. Experiments are conducted in a horizontal tube with an inner diameter of 32 mm, where a partial condensation in stratified flow occurs. The results challenge the common assumption of thermodynamic equilibrium as the measured local saturation temperature deviates from its calculated value. Heat transfer coefficients for two different compositions are reported in a range of 500 $W\,m^{-2}\,K^{-1}$ to 1100 $W\,m^{-2}\,K^{-1}$, showing clear trends against vapour quality, mass flux and pressure. The differentiation between temperature measurement and calculation has a large impact that clearly outweighs reported measurement uncertainties from the sensor equipment. Differences in the resulting heat transfer coefficients partly exceed 20 %, depending on the operating conditions. The deviation is further increased under consideration of fitted interaction parameters, even though the impact is comparable smaller and lies in the range of measurement uncertainties. The obtained results clarify possible sources of deviations between different experimental studies.

1. Introduction

A growing interest in applications of thermodynamic cycles has been seen in recent years due to the importance of high-efficiency and environmental-friendly energy systems. In addition to development on a component basis, much research has been done in the field of working fluids. While sporadically discussed earlier, zeotropic mixtures have been investigated for their application in thermodynamic cycles starting in the 1980s [1–5]. Mostly, two aspects have driven the interest in zeotropic mixtures despite an increased handling effort. Firstly, by varying the composition of a given mixture, the fluid properties can be adjusted. Depending on the application, a best-fitting mixture can be found based on its properties. Secondly, matching the temperature glide of a mixture during its phase change process to the temperature difference of a heat source or sink increases the second-law efficiency of the heat transfer. The consequence is better use of the exergy available to the system. This concept has been investigated multiple times, especially in refrigeration, heat pumps, and low-temperature power cycles [6–8]. Latter of these cases represents the Organic Rankine Cycle (ORC) that can be used to generate electricity from low-temperature energy sources or waste heat. Still, zeotropic mixtures were described by worse heat transfer characteristics in comparison to their respective pure components [9]. The advantage of more efficient cycles has to be

* Corresponding author.
E-mail address: clemens.berger@uni-bayreuth.de (C. Berger).

https://doi.org/10.1016/j.expthermflusci.2026.111760
Received 13 November 2025; Received in revised form 24 March 2026; Accepted 22 April 2026
Available online 24 April 2026

Nomenclature

Symbols

α	Reduced Helmholtz energy, –
β	HEOS interaction parameter, –
γ	HEOS interaction parameter, –
δ	Reduced mixture density, –
θ	HEOS interaction parameters, –
ρ	Density, $\mathrm{kg\,m^{-3}}$
$\underline{\rho}$	Molar density, $\mathrm{mol\,m^{-3}}$
τ	Inverse reduced temperature, –
A	Scalar input variable, –
B	Scalar output variable, –
D	Diameter, m
G	Mass flux, $\mathrm{kg\,m^{-2}\,s^{-1}}$
h	Heat transfer coefficient, $\mathrm{W\,m^{-2}\,K^{-1}}$
i	Specific enthalpy, $\mathrm{kJ\,kg^{-1}}$
i_{fg}	Specific enthalpy of vaporisation, $\mathrm{kJ\,kg^{-1}}$
j	Iterative number, –
k	Thermal conductivity, $\mathrm{W\,m^{-1}\,K^{-1}}$
L	Length, m
l	Iterative number, –
$\dot{m}$	Mass flow rate, $\mathrm{kg\,s^{-1}}$
n	Number, –
P	Power, W
p	Pressure, kPa
$\tilde{p}$	Probability, –
p^*	Reduced pressure, –
$\dot{Q}$	Heat flow rate, W
$\dot{q}$	Heat flux, $\mathrm{W\,m^{-2}}$
R	Molar gas constant, $\mathrm{J\,mol^{-1}\,K^{-1}}$
T	Temperature, K
U	Expanded measurement uncertainty, –
u	Combined standard uncertainty, –
v	Molar volume, $\mathrm{m^3\,mol^{-1}}$
X	Mole concentration, $\mathrm{mol\,mol^{-1}}$
x	Vapour quality, –
z	Mass concentration, $\mathrm{kg\,kg^{-1}}$
var	Variance, –

Superscripts and subscripts

bubble	Bubble point
c	Critical
i	Inner
id	Ideal
imc	Intermediate cycle
in	Inlet
l	Saturated liquid phase
meas	Measured value
o	Outer
out	Outlet
pc	Precondenser
R	Refrigerant
r	Reduced value
sat	Saturated state
ts	Test section
v	Saturated vapour phase
W	Water
w	Wall

Abbreviations

DAQ	Data acquisition system
GEMC	Gibbs Ensemble Monte Carlo
GWP	Global warming potential
HCFO	Hydrochlorofluoroolefin
HEOS	Helmholtz equation of state
HFO	Hydrofluoroolefin
HTC	Heat transfer coefficient
MCMC	Markov Chain Monte Carlo
ORC	Organic Rankine cycle
VLE	Vapour-liquid equilibrium

evaluated against the need for larger sizing of heat transfer equipment. The correlations used to calculate heat transfer coefficients (HTC) during the design of thermodynamic cycles usually match a broader collection of experimental heat transfer data in the range of ±20 % [10–12]. This illustrates the challenge of improving the accuracy of heat transfer measurements and the derived correlations.

Comparing both evaporation and condensation heat transfer, experimental investigations usually yield lower uncertainties in the HTC for evaporation. That is due to electrical heating as power input. Condensation is more dependent on an appropriate set-up to determine the transferred heat. The most common approach for in-tube condensation is the evaluation by an enthalpy profile method [13]. It refers to the enthalpy difference due to heating of the cooling medium which is quantified by temperature and pressure measurements. The resulting heat flow rate is assumed to be identical to the condensation heat flow rate under assumption of an adiabatic system. Condensation in horizontal tubes has been investigated in relevance to various thermodynamic cycle systems by measurements in a coaxial tube-in-tube test section. The cooling medium circulates in counterflow orientation to the working fluid and absorbs the ejected heat. Two main approaches to an experimental set-up can be found in literature, covering the large majority of all studies.

The first approach is based on the realisation of a total condensation. Superheated vapour is led to a test section where the working fluid is condensed and subcooled. A segmentation of the overall test section enables the determination of HTCs for the partial condensation with varying vapour qualities in different subsections. Jacob and Fronk [14] investigated the working fluid R1233zd(E) with a low global warming potential (GWP), which belongs to the group of hydrochlorofluoroolefins (HCFO), with respect to its heat transfer characteristics for ORC condensers. The horizontal tube-in-tube test section with an inner diameter of 4.7 mm was 1.6 m in length to ensure a total condensation. It was segmented into seven parts by the cooling water cycle. For each section, the mean HTC was determined along the vapour quality. The heat duty was measured by the enthalpy profile in these sections. Thermodynamic equilibrium was assumed in the flow so that local temperatures could be calculated by enthalpy and pressure. Across all operating conditions, the authors reported a maximum uncertainty of 15.1 % for the HTC. Condensation of R134a was investigated by Azzolin et al. [15] with a small modification of the method. Due to higher accuracy, differential pressure sensors were used across five sub-sections so that local pressures were indirectly determined. The authors reported uncertainties of up to 7.1 % for condensation in a horizontal tube at a mass flux of $50\,\mathrm{kg\,m^{-2}\,s^{-1}}$.

Total condensation of a fluid mixture was conducted by Mazumder et al. [16] for R32/R1234ze(E) to determine heat transfer coefficients. The test section was divided into twelve subsections with measurements of the enthalpy profile of cooling water. The mixture temperature glide

was determined via temperature measurements with thermocouples at specific locations that, however, did not match the length of single test sections. The authors did not comment on their procedure in depth, but local fluid temperatures for HTC calculations had to be interpolated or calculated again by their formulation in dependency of pressure and enthalpy. The resulting HTCs were evaluated against different pure fluid correlations with additional mixture models. The better matching correlations achieved mean deviations of about 15 % to the experimental data, while being very accurate especially at higher mass fluxes. A similar mixture R32/R1234yf was applied by Wang et al. [17], the condensation tube with an inner diameter of 4 mm was 3.4 m in length. The segmentation into five subsections was done in a way so that spacings of 0.2 m were in between them. Locally measured refrigerant temperatures were compared to the vapour-liquid interface temperature and the vapour bulk temperature obtained from a non-equilibrium calculation model. In the range of vapour qualities $0.2 < x < 0.8$, the results showed good agreement. The measured fluid temperature exceeded the predicted one at low vapour qualities, but was lower at high vapour qualities. It has to be noted that the saturation temperature in measurements was not reported to be measured but rather calculated by pressure and vapour quality. Consequently, the measured temperature should be evaluated as theoretical value under assumption of thermodynamic equilibrium.

Measurements of the refrigerant temperature during total condensation in a test section were proven to be implementable by Lee and Son [18]. The authors built a test section with ten subsections for heat transfer while keeping small adiabatic distances in between. There, the local condensation temperatures were measured by installed thermocouples. HTCs were determined for different tube sizes and operational conditions. The condensation flow was observed to change from annular to stratified wavy flow depending on mass flux and vapour quality. This in mind, the sensor position has to be chosen carefully as the spatial partition of the phases changes. The resulting HTCs were the highest during condensation in the tube with the smallest diameter, increasing also with mass flux and annular flow. In another study, Moreira et al. [19] positioned thermocouples inside bulbs fused to the tube in order to measure the refrigerant side temperature. While requiring additional effort in manufacturing and consideration of the missing direct contact between fluid and sensor, this methods allows for temperature measurement at any position without adiabatic intersections.

The second approach to measurements of the condensation heat transfer in horizontal tubes is based on a partial condensation within a test section. By that, the vapour quality has to be adjustable to variable values. The effort of experimental campaigns is generally higher due to one operating point not yielding HTCs for different state points. However, local measurements of temperature and pressure at inlet and outlet of the test section in addition to precise statement of a mean vapour quality allow for more accurate results. An early set-up for partial condensation was proposed by Dobson et al. [20] for comprehensive measurements of the condensation process. The state at the test section inlet was set by an electrical heater to partially evaporate the liquid flow. Evaluation of HTCs for annular and stratified flow was carried out and an often used correlation was derived. Vapour quality setting by partial evaporation was also done in [21,22]. These works did not include wall temperature measurements but rather used the logarithmic mean temperature difference between refrigerant and cooling water sides to calculate the total HTC. From this value, the condensation HTC was derived but reported with uncertainties up to about 15 % in both cases. Further studies conducting a partial condensation [23–25] implemented additional heat exchangers to set specific state points in the test section. Forcing superheated vapour through a precondenser, the refrigerant was partially condensed. The vapour quality at precondenser outlet and thus test section inlet could be obtained from the enthalpy profile of cooling water. Local refrigerant temperatures were measured at inlet and outlet of the test section so that HTCs were calculated in dependency of the mean vapour quality within the test section.

One major point of discussion in this measurement approach is the averaging of HTCs and vapour qualities. In order to use this assumption reliably, the change of vapour quality in the test section must be limited and the wall temperature must be quasi-constant over the heat exchanger length. The latter condition causes the temperature difference between wall and fluid to be constant, the expression that is used to calculate the HTC. Garimella and Bandhauer [26] and Bandhauer et al. [27] were first to propose a two-stage cooling cycle in order to achieve these conditions. The principle deploys two different cycles filled with cooling water. The first of them is connected to the condensation test section and absorbs heat from the refrigerant. In this cycle, the mass flow rate of water is set to high values, resulting in low temperature differences and thus a quasi-constant wall temperature. The cooling water is instead connected to a secondary cycle by another heat exchanger, which is equipped with sensors to determine the heat flow rate ejected by the refrigerant. The authors proposed this method as so-called thermal amplification technique in studies of condensation in microchannels. In this instance, the overall heat duty is especially low and thus harder to accurately measure. In the application of the thermal amplification technique, additional effort had to be done in order to consider thermal losses and input from the primary cooling cycle.

The thermal amplification technique was later used by Ghim and Lee [28,29] for condensation measurements in a horizontal tube with an inner diameter of 7.75 mm. The change of vapour quality over the test section length was at 0.15 at maximum. Uncertainties of up to 25 % for HTCs at lower vapour qualities were reported despite the additional effort. This illustrates that the qualitative effect of calculating quasi-constant HTCs does not necessarily reflect in quantitative assessment of measurement uncertainties.

From the published studies on condensation heat transfer, two ways of fluid temperature determination have emerged. If possible at a given set-up, the temperature may be measured. If not, calculation in dependency of pressure and vapour quality under assumption of thermodynamic equilibrium has to be done. In most cases, especially for condensation of pure fluids, the differences vanish. Fronk and Garimella [9] proposed the definition of a real and an apparent HTC value on a basis of the temperature definition. The first term refers to the measurement of a bulk vapour temperature, while the second one refers to the calculated temperature. Latter of these values is more feasible in its determination but yields less realistic HTC results. It is therefore used if the experimental set-up does not allow for local fluid temperature measurements. The authors linked this differentiation to zeotropic mixtures where the temperature glide in combination with mass transfer resistances causes non-equilibrium conditions to prevail. In a later work [30], they also defined an actual liquid HTC. The interface temperature between the liquid and vapour phase, however, is not feasible to measure for its determination. From these different definitions, the need for an statement of the used temperature in experimental studies is clearly given. This could answer the question of what the impact of different methodologies realistically is.

In this study, the potential impact of the design and calculation methods of condensation heat transfer measurements is assessed. Three different aspects are investigated during experiments on the in-tube condensation of the zeotropic mixture R134a/R1233zd(E). The main aspect is fluid temperature definition in the calculation of HTCs. Measurement at inlet and outlet of the test section as well as calculation in dependency of pressure and vapour quality yield the real and apparent HTC, respectively. Two peculiarities of this study enhance the effect to have a greater influence, which are the application of a zeotropic mixture, that causes temperature gradients in the test section, and a flow stratification at low mass fluxes that would originate from part load operation of an ORC or heat pump. The second aspect is related to averaging of vapour quality and HTC during experiments

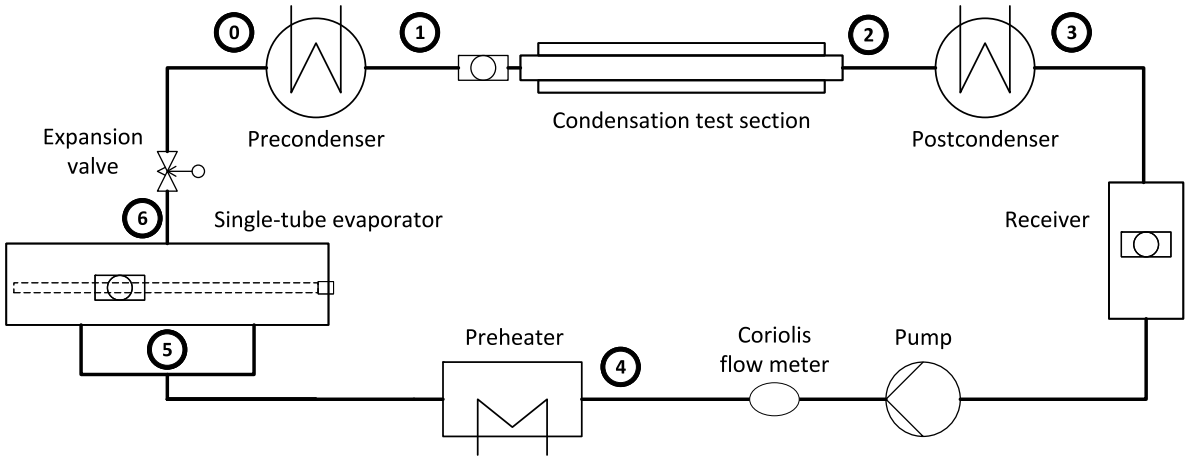

Fig. 1. Schematic of the mixture cycle in the utilised ORC test rig.

covering a partial condensation. A thermal amplification technique, which has been proposed in the literature, is used for the present study. Its impact is assessed by a measurement uncertainty evaluation of the resulting HTC. The third effect to be analysed is the propagation of uncertainties in relation to the modelling of thermophysical properties by the Helmholtz Equations of State (HEOS). For pure fluids, HEOS parameters are well established, but mixtures require additional "mixing" parameters that must either be fitted to experimental data or, in their absence, are estimated from similar systems. This is the case for the given mixture R134a/R1233zd(E) for which the default interaction parameters in REFPROP 10 [31] are transferred from the mixture R1234yf/R134a. Yet the accuracy of this transfer remains essentially unknown. Whenever vapour–liquid equilibrium (VLE) data is available, mixture-specific interaction parameters can be fitted directly. Such data may come from laboratory measurements or be generated via molecular simulations ("synthetic measurements"). Because the VLE data themselves carry experimental or statistical uncertainties, the resulting interaction parameters are also uncertain. In this work, we quantify how uncertainties in these mixture parameters – here exemplarily derived from molecular simulation – propagate into subsequent calculations of heat transfer coefficients and thermodynamic state points.

These stated aspects to be investigated are evaluated against quantified measurement uncertainties originating from sensor equipment. Data is recorded for two different concentrations of mixture components that yield mean temperature glides of 6 K and 9 K. The vapour quality within the test section ranges between 0.25 and 0.85. Condensation is observed at different pressure levels in the range 220 kPa to 340 kPa corresponding to condensation temperatures from 37 °C to 52 °C and different mass fluxes 40 $\mathrm{kg\,m^{-2}\,s^{-1}}$ to 80 $\mathrm{kg\,m^{-2}\,s^{-1}}$. The impact of these influencing parameters on resulting condensation HTCs and the analysed aspects of measurement design is quantified and discussed.

2. Experiments

2.1. Experimental facility

The experimental investigations in this study are carried out with an existing ORC test rig built for experimental investigations of pool boiling heat transfer and power output [32,33], which has been expanded by the condensation test section. The tube diameter was derived from a geothermal power plant driving an ORC for power generation. A schematic of the cycle and its containing components is shown in Fig. 1. The refrigerant flow is driven by a piston diaphragm pump G03 by manufacturer Verder Liquids. The preheater is the electrically powered flow heater Elmess HF/SE-7. It has a separated temperature control with its target values being set to 1 K below saturation temperature during operation. The evaporator is a unique component designed and manufactured for pool boiling heat transfer measurements [34]. The cylindrical vessel has a volume of 8 L and is equipped with an electrically heated copper tube. Evaporation in the given ORC set-up is limited to 120 °C and 1300 kPa. The maximum power output of the tube is 14.4 kW, the nominal value during operation

$$P = i_{\mathrm{fg}}\,\dot{m}_{\mathrm{R}} \tag{1}$$

determines depending on the enthalpy of vaporisation i_{fg} the circulating refrigerant mass flow rate $\dot{m}_{\mathrm{R}}$. High pressure vapour is led through an expansion device to reduce the system pressure on the condensation side. The condensation section consists of three different heat exchangers but will be explained in detail in the following section. The installed receiver accumulates excess refrigerant charge.

In order to meet specific requirements regarding the aim of this study as well as general operational aspects, the investigated mixture R134a/R1233zd(E) was carefully chosen. The mixture prerequisites are:

1. A temperature glide $\Delta T > 5$ K,
2. No fitted binary interaction parameters in the fluid property database,
3. Condensation temperatures and pressures adequate to the ORC system,
4. An as low as possible environmental impact,
5. No flammable components.

A first categorisation of possible mixture components is made by points 3 to 5. The mixture must be applicable to the ORC operating range where condensation in the range 20 °C to 60 °C occurs at pressures below 700 kPa. Non-flammable fluids with a low global warming potential (GWP) and negligible ozone depletion potential are present in the group of hydrofluoroolefins (HFOs) and HCFOs. The refrigerant R1233zd(E) is nowadays state-of-the-art in applications of ORC and high temperature heat pump systems and will be used as main component in this study. However, its mixtures with other fluids of the HFO group do not show large differences in saturation temperatures. The resulting temperature glide during isobaric phase change would not meet the given requirement. Instead, R134a is chosen as secondary component with low mass fractions below 10 %. The mixture R134a/R1233zd(E) is not commonly used in literature and application but finally chosen for this study as it meets all stated requirements. The circulating mass fraction of R134a is 5 % and 7 % in the different compositions. An overview of chosen properties for the mixture components is given in Table 1.

Table 1
Fluid properties of the mixture and its components at 200 kPa.
Source: Data from [31].

Component	p_c/kPa	T_c/°C	T_l/°C	T_v/°C	ρ_l/kg m^{-3}	ρ_v/kg m^{-3}	i_{fg}/kJ kg^{-1}	GWP [35]
R134a	4059.3	101.06	−10.08	−10.08	1327.4	10.0	206.02	1430
R1233zd(E)	3623.7	166.45	37.68	37.68	1231.5	10.9	184.35	3.88
0.05 R134a/0.95 R1233zd(E)	3746.3	163.17	29.29	35.92	1249.3	10.8	192.56	75.2
0.07 R134a/0.93 R1233zd(E)	3791.4	161.84	26.54	35.20	1255.0	10.7	195.12	103.7

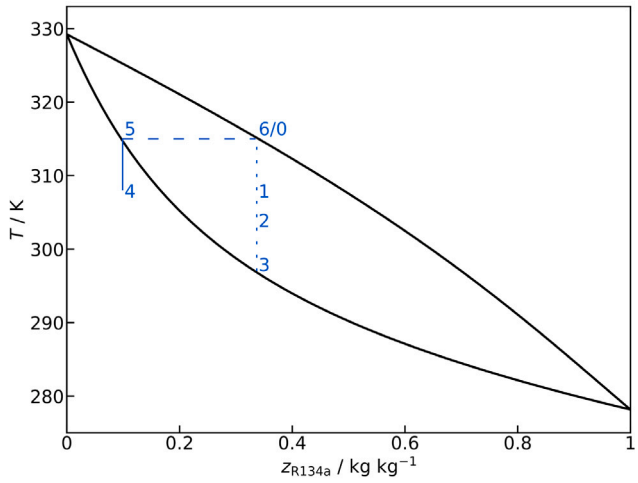

Fig. 2. VLE of the mixture R134a/R1233zd(E) at 350 kPa.

A peculiarity in the interaction between the chosen mixture and the experimental set-up must be addressed. Component separation in two-phase flow during phase change causes an phenomenon where the global circulating composition differs from the filled composition in most cases. The main reason for this is liquid hold-up in two-phase regions of heat exchangers and liquid receivers. Only in the instance of minimal heat exchanger volume and absence of receivers, composition shift can be neglected. This effect was first calculated by Chen and Kruse [36]. As a consequence, the circulating composition of zeotropic mixture flow must somehow be determined. Looking at the given set-up, a much more dominant cause of composition shift has to be considered. This is the evaporator, in which a separation between liquid and vapour phase occurs. Liquid refrigerant is hold back at all time so that the heated tube is flooded. The vapour phase exits the vessel at the top and enters the cycle.

The vapour-liquid equilibrium curve at 350 kPa is shown in Fig. 2 considering all state points from Fig. 1. Subcooled liquid of the initial composition at point 4 is heated to bubble point temperature at point 5. Considering isothermal conditions in the evaporator due to the installed preheater, the separation potential causes the composition difference Δz between liquid and vapour phase (5 → 6). The amount of this composition adjustment is way higher than expected composition shift without a flooded evaporator. Having filled only 1 % of R134a in mass fraction, the circulating mixture contains about 5 %. During condensation (0 → 3), the composition does not change but the temperature glide evokes a temperature gradient. Note, that the VLE is only drawn for one specific pressure, whereas evaporation and condensation occur on different pressure levels in experiments. The effect of composition adjustment within the evaporator is intendedly used to specify the condensing mixture. Filling less R134a lowers the effective GWP while the adjustment evokes a measurable temperature glide of at least 5 K.

2.2. Condensation section

With the heat transfer test section being designed to conduct a partial condensation, the overall condensation section contains two heat exchangers connected to the working fluid cycle in addition to the test section itself. All equipment is insulated, so that adiabatic conditions are assumed in the measurement evaluation. A schematic of the condensation section is shown in Fig. 3, depicting all installed components and sensors. The precondenser is a plate heat exchanger (B12Lx40) by manufacturer SWEP which is used to cool superheated vapour (state 0) to bubble point temperature and further conduct a partial condensation at test section inlet (state 1). The postcondenser is another plated heat exchanger (B10THx40) by SWEP, installed inline behind the test section outlet (state 2). Its purpose is the complete condensation and subcooling of the liquid mixture. Both plated heat exchangers are connected to the laboratory's cooling water supply. The water flow rate is adjusted by pneumatic valves to control the condensation pressure level. An increase of the water flow rate results in lower pressures in the working fluid cycle. The water lines are instrumented with pressure, temperature and flow rate sensors to determine the energy balance and thus transferred heat flow rate.

Before entering the test section, the refrigerant passes through a cylindrical sight glass. Stratified flow is observed under all operating conditions. The test section is a $L = 1.2$ m long tube-in-tube heat exchanger designed and built at the University of Bayreuth. The inner tube, where condensation is conducted, has an inner diameter of $D_{w,i} = 32$ mm and an outer diameter of $D_{w,o} = 36$ mm. In the annulus between inner and outer tube ($D_o = 53$ mm), water is circulating in counter-current orientation to the refrigerant side. The test section is manufactured of stainless steel 1.4301. Temperature and pressure are measured at inlet and outlet on the refrigerant side. Additionally, the wall temperature is measured at in total 16 locations. There are 2 positions in distance of 0.4 m from inlet and outlet, at which 8 thermocouples are placed uniformly around the perimeter. The sheathed thermocouples are attached to the outer wall of the inner tube with a perpendicular orientation. This positioning is depicted in Fig. 4.

The test section water side consists of a two-stage cycle system with additional components. It enables the determination of HTCs under the thermal amplification technique. A high flow rate driven by the circulation pump (Pedrollo DHL 25-60/130) in the primary cooling cycle lowers the water temperature change due to heat absorption. This minimises gradients in the test section and allows for the assumption of quasi-constant wall temperature but consequences high uncertainties in temperature and thus heat flow rate measurements. This mismatch is solved by the two-stage cycle design. The water, which remains connected to the test section, is enclosed in a loop, making the primary cooling cycle an intermediate one. It is connected via a plated heat exchanger (SWEP B8Lx6) to the secondary water cycle. There, a low water flow rate is maintained during operation with measurement of the mass flow rate, pressure and temperature. The secondary cycle itself is coupled to a process chiller (VC 2000) by manufacturer LAUDA. Lowering the set point temperature of this process chiller, the water temperature of the intermediate cycle also decreases. In this way, the heat flow rate and change of vapour quality over the test section can be adjusted.

2.3. Experimental procedure

Three parameters are observed with respect to their influence on the condensation HTC. The vapour quality x can be set to specified values in a range between 0.25 and 0.85 in the test section. The adjustment is

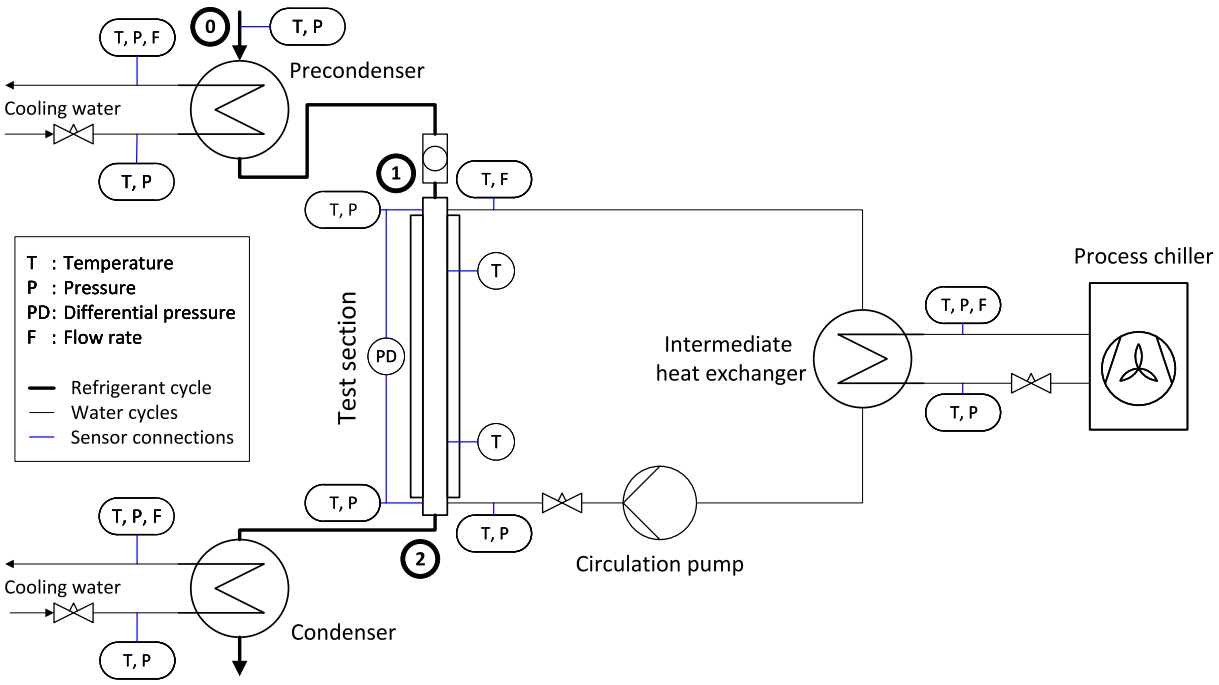

Fig. 3. Schematic of the condensation section with components and sensors.

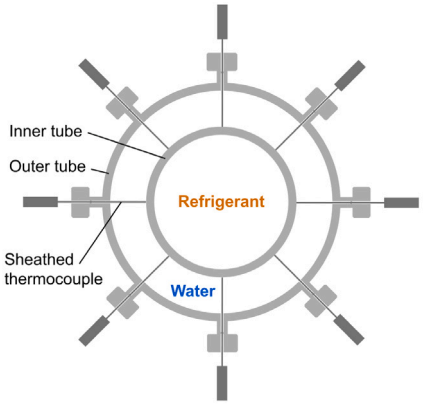

Fig. 4. Cross section view of the test section with thermocouple placement.

carried out by variation of the water flow rate in the line connected to the precondenser. Higher flow rates cause increased heat flow rates and thus lower values of the vapour quality. Resulting from the comparably large tube diameter, the mass flux G is kept at low values in the range $40\,\mathrm{kg\,m^{-2}\,s^{-1}}$ to $80\,\mathrm{kg\,m^{-2}\,s^{-1}}$. This results in a stratification in the flow where the vapour flows on top of the liquid phase. The pressure of the condensing mixture is dependent on the overall temperature of cooling water. By increasing the flow rate of cooling water in the cycles coupled with precondenser and postcondenser, the water temperature change is lowered. Resulting from that, the condensation pressure decreases. The pressure is evaluated by means of the reduced pressure $p*$, where the actual pressure is set in relation to the mixture critical pressure. The critical pressure is dependent on the composition and retrieved from a REFPROP spline calculation.

Measurements are each carried out over a time span of ten minutes in stationary operation where all sensor data is recorded every two seconds. This procedure allows for time averaging the results in later calculations, minimising effects of sensor noise and unintended fluctuations. The requirements for stationary conditions are:

1. No change in the measured liquid level of the receiver besides signal noise,
2. Deviations of the mean condensation pressure of less than 1 kPa from the target value,
3. Limited fluctuations in the condensation pressure so that the deviation between minimum and maximum value are below 1 kPa.

The last requirement is of great importance as the two-stage cooling cycle introduces additional inertia to the system. Furthermore, the deviations of vapour quality and mass flux from set points are observed. The mean vapour quality, which is calculated from state points 1 and 2, has a deviation of less than 0.01 to its target values under most operating conditions. Due to it being highly sensitive to mixture composition and time averaging, the maximal accepted deviation is at 0.02. This holds also for the difference between maximal and minimal vapour quality for measurement series with varying pressure or mass flux. The mixture mass flow rate, which is measured by a Coriolis type sensor, exhibits greater fluctuations resulting from the pump characteristics. A deviation of $5\,\mathrm{kg\,m^{-2}\,s^{-1}}$ in the resulting mass flux is accepted in this study.

3. Mixture modelling

3.1. Helmholtz equation of state

The data processing in Section 4 requires several calculations of thermodynamic properties which are usually done in the form of the reduced Helmholtz energy

$$\alpha = \frac{a}{RT} = \alpha^{(\mathrm{id})}(\underline{\rho}, T, \boldsymbol{X}) + \alpha^{(\mathrm{r})}(\tau, \delta, \boldsymbol{X}), \tag{2}$$

that is split into the ideal reduced free-energy $\alpha^{(\mathrm{id})}$ and the residual reduced free-energy part $\alpha^{(\mathrm{r})}$. Mixtures are modelled as a combination of the pure component HEOS using mixture models based on binary interaction parameters fitted to experimental data. Introduced by Lemmon and Tillner-Roth [37] and further refined by Kunz and Wagner [38] the reduced Helmholtz energy is given by

$$\alpha^{(\mathrm{r})}(\tau, \delta, \boldsymbol{X}) = \sum_{j=1}^{N} X_j \alpha_{0j}^{(\mathrm{r})}(\tau, \delta) + \alpha_{\mathrm{dep}}^{(\mathrm{r})}. \tag{3}$$

The sum in Eq. (3) collects the corresponding state contributions $\alpha_{0j}^{(r)}$ of the reduced Helmholtz energy weighted by the component mole fractions X_j. The second part $\alpha_{dep}^{(r)}$ is the departure function.

The interaction parameters are used in the reduced mixture density δ and the inverse reduced mixture temperature τ, which are given by

$$\delta = \frac{\rho}{\underline{\rho}_r(\boldsymbol{X})} \quad \text{and} \quad \tau = \frac{T_r(\boldsymbol{X})}{T}. \tag{4}$$

The composition dependent reducing functions weight the components' critical molar densities or corresponding molar volumes $v_{c,i}$ and the components' critical temperatures as

$$\frac{1}{\underline{\rho}_r} = v_r = \sum_{j=1}^{N} X_j^2 v_{c,j} + \sum_{j=1}^{N-1}\sum_{l=j+1}^{N} 2X_j X_l v_{jl} \frac{X_j + X_l}{\beta_{v_{jl}}^2 X_j + X_l} \tag{5}$$

$$\text{with} \quad v_{jl} = \frac{1}{8}\beta_{v_{jl}}\gamma_{v_{jl}}\left(v_{c,j}^{\frac{1}{3}} + v_{c,l}^{\frac{1}{3}}\right)^3 \tag{6}$$

and

$$T_r = \sum_{j=1}^{N} X_j^2 T_{c,j} + \sum_{j=1}^{N-1}\sum_{l=j+1}^{N} 2X_j X_l T_{jl} \frac{X_j + X_l}{\beta_{T_{jl}}^2 X_j + X_l} \tag{7}$$

$$\text{with} \quad T_{jl} = \beta_{T_{jl}}\gamma_{T_{jl}}\sqrt{T_{c,j}T_{c,l}}. \tag{8}$$

The software library REFPROP 10 [31] implements several HEOS for pure substances and certain mixtures. However, to the best knowledge of the authors, for the mixture R134a/R1233zd(E) measurement data required to fit the interaction parameters is not available. Thus, they are not implemented in the software and can only be inferred using simplified mixing rules.

3.2. Parameter fitting

In order to retrieve more reliable mixture interaction parameters, VLE data of the zeotropic mixture R134a/R1233zd(E) are required. For doing so, molecular simulations can be performed [39]. In order to obtain the required VLE data for the mixture at hand, Gibbs-Ensemble-Monte-Carlo (GEMC) simulations have been carried out, the details of which can be found in Appendix A.

The simulations result in predicted phase compositions $X^{(\text{dew/bubble})}$ and saturated phase densities $\rho^{(\text{dew/bubble})}$. While equivalent measurement data would be subject to measurement uncertainties, GEMC simulations yield uncertainty estimates by repetitions of simulations under different initial configurations. Projecting the uncertainties in the GEMC data as well as finding the correct mixing parameters can be accomplished by Bayesian parameter fitting [40]. In order to do so, the model

$$\left(X_i^{(\text{dew})}, X_i^{(\text{bubble})}, \rho_i^{(\text{dew})}, \rho_i^{(\text{bubble})}\right)^\intercal = \boldsymbol{f}_{\text{fl}}(T_i, p_i, \boldsymbol{\theta}), \quad i = 1, \dots, N \tag{9}$$

is introduced, where the flash algorithm calculates the phase compositions and densities for a certain pressure p_i and temperature T_i given the interaction parameters $\boldsymbol{\theta}$. As only VLE data are available, the parameters $\boldsymbol{\theta} = (\beta_T, \gamma_T)^\intercal$ will be calibrated as suggested by Bell and Lemmon [41]. The departure function is neglected and the remaining parameters are set to $\beta_v = \gamma_v = 1$.

A Bayesian approach is used to infer the uncertainties in the interaction parameters, based on the VLE data. Thus, $\boldsymbol{\theta}$ is modelled as a random vector and embedded in the data model

$$\left(\tilde{X}_i^{(\text{dew})}, \tilde{X}_i^{(\text{bubble})}, \tilde{\rho}_i^{(\text{dew})}, \tilde{\rho}_i^{(\text{bubble})}\right)^\intercal = \boldsymbol{f}_{\text{fl}}(T_i, p_i, \boldsymbol{\theta}) + \boldsymbol{\epsilon}_i, \quad i = 1, \dots, N, \tag{10}$$

with the independent Gaussian noise elements

$$\boldsymbol{\epsilon}_i \sim \mathcal{N}\left(\boldsymbol{0}, \text{diag}\left(\text{var}_{X,i}^{(\text{dew})}, \text{var}_{X,i}^{(\text{bubble})}, \text{var}_{\rho,i}^{(\text{dew})}, \text{var}_{\rho,i}^{(\text{bubble})}\right)\right). \tag{11}$$

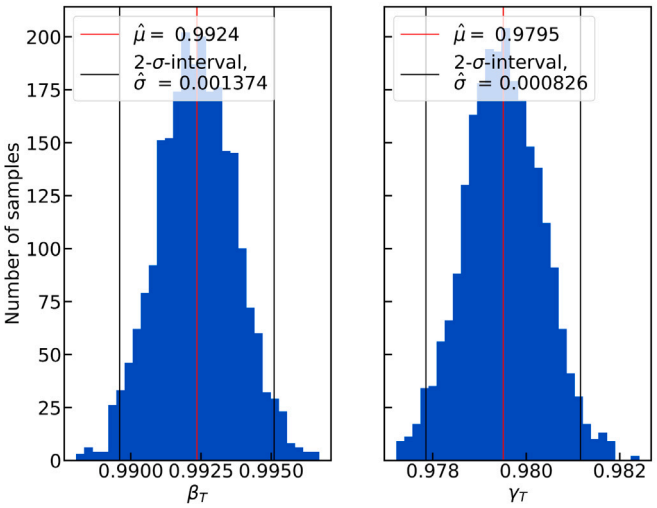

Fig. 5. Histogram of MCMC interaction parameter samples.

The conditional density of the interaction parameters $\boldsymbol{\theta}$ given the data $\mathcal{D}_i = \left(\tilde{X}_i^{(\text{dew})}, \tilde{X}_i^{(\text{bubble})}, \tilde{\rho}_i^{(\text{dew})}, \tilde{\rho}_i^{(\text{bubble})}, T_i, p_i\right)^\intercal$ can be calculated as

$$\underbrace{\pi(\boldsymbol{\theta} \mid \mathcal{D})}_{\text{posterior}} \propto \underbrace{\pi\left(\tilde{\boldsymbol{X}}^{(\text{dew})}, \tilde{\boldsymbol{X}}^{(\text{bubble})}, \tilde{\boldsymbol{\rho}}^{(\text{dew})}, \tilde{\boldsymbol{\rho}}^{(\text{bubble})} \mid \boldsymbol{p}, \boldsymbol{T}, \boldsymbol{\theta}\right)}_{\text{likelihood}} \cdot \underbrace{\pi(\boldsymbol{\theta})}_{\text{prior}}, \tag{12}$$

using Bayes theorem, where the data is denoted in vectorial form. Given the uncorrelated Gaussian noise model, the likelihood can be calculated as

$$\begin{aligned}&\pi\left(\tilde{\boldsymbol{X}}^{(\text{dew})}, \tilde{\boldsymbol{X}}^{(\text{bubble})}, \tilde{\boldsymbol{\rho}}^{(\text{dew})}, \tilde{\boldsymbol{\rho}}^{(\text{bubble})} \mid \boldsymbol{p}, \boldsymbol{T}, \boldsymbol{\theta}\right) \\ &\quad = \pi\left(\tilde{\boldsymbol{X}}^{(\text{dew})} \mid \boldsymbol{p}, \boldsymbol{T}, \boldsymbol{\theta}\right) \pi\left(\tilde{\boldsymbol{X}}^{(\text{bubble})} \mid \boldsymbol{p}, \boldsymbol{T}, \boldsymbol{\theta}\right) \\ &\quad\quad \pi\left(\tilde{\boldsymbol{\rho}}^{(\text{dew})} \mid \boldsymbol{p}, \boldsymbol{T}, \boldsymbol{\theta}\right) \pi\left(\tilde{\boldsymbol{\rho}}^{(\text{bubble})} \mid \boldsymbol{p}, \boldsymbol{T}, \boldsymbol{\theta}\right)\end{aligned} \tag{13}$$

with normally distributed

$$\pi(\boldsymbol{\rho}^{(\text{dew/bubble})} \mid \boldsymbol{p}, \boldsymbol{T}, \beta_T, \gamma_T) \sim \mathcal{N}\left(\boldsymbol{X}^{(\text{dew/bubble})} \mid \boldsymbol{\Sigma}_X^{(\text{dew/bubble})}\right) \tag{14}$$

and

$$\pi(\boldsymbol{X}^{(\text{dew/bubble})} \mid \boldsymbol{p}, \boldsymbol{T}, \beta_T, \gamma_T) \sim \mathcal{N}\left(\boldsymbol{\rho}^{(\text{dew/bubble})} \mid \boldsymbol{\Sigma}_\rho^{(\text{dew/bubble})}\right), \tag{15}$$

where the covariance matrices are given by

$$\boldsymbol{\Sigma}_X^{(\text{dew/bubble})} = \text{diag}\left(\text{var}_{X,1}^{(\text{dew/bubble})}, \dots, \text{var}_{X,N}^{(\text{dew/bubble})}\right) \tag{16}$$

$$\text{and} \quad \boldsymbol{\Sigma}_\rho^{(\text{dew/bubble})} = \text{diag}\left(\text{var}_{\rho,1}^{(\text{dew/bubble})}, \dots, \text{var}_{\rho,N}^{(\text{dew/bubble})}\right). \tag{17}$$

As the posterior in Eq. (12) is difficult to calculate in closed form, a Markov Chain Monte Carlo (MCMC) method is used to sample from it. In particular, the Affine Invariant Ensemble Sampler introduced by Goodman and Weare [42] implemented in the Python package emcee [43] is used. Sampling was done with 20 walkers for 5000 steps each. A burn-in of 200 and thinning, i.e. keeping only 1 out of 40 consecutive samples, was applied. Histograms of the remaining 2400 samples are shown in Fig. 5.

Using the estimated mean values, the HEOS parameters can be updated to achieve more accurate mixture property modelling. The fitted model in conjunction with the GEMC data is shown in Fig. 6. Using the samples, the effect of uncertainties in the property calculations will be evaluated in the following sections.

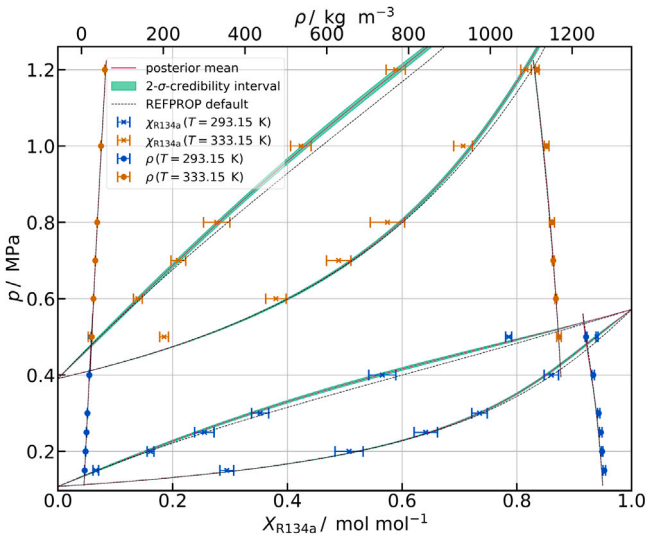

Fig. 6. GEMC VLE simulation results and fitted HEOS model for molar compositions and densities together with 2-σ-credibility intervals in comparison to REFPROP predictions using default interaction parameters.

4. Data processing

4.1. Calculation methods

4.1.1. Circulating mixture composition

Due to the vapour-liquid separation within the evaporator, the circulating composition of the mixture R134a/R1233zd(E) depends on the evaporation pressure and thus changes between all operating points. The composition entering the condensation section at state **0** is equal to the composition at state **3** and is determined for each measurement by calculation of the VLE data. Local measurements of the saturation temperature and pressure in direct fluid contact within the evaporator yield information about the bubble point. The temperature value is assumed to represent the local bubble point temperature. In preliminary tests for pure R1233zd(E), this has proven to be valid, as the deviation between temperature measurement and data retrieved from REFPROP did not exceed 0.1 K under any condition. By minimising the function

$$\Delta T = |T_{\mathrm{meas}} - T_{\mathrm{bubble}}(p_{\mathrm{meas}}, z)|, \tag{18}$$

the circulating composition is determined for each operating point. Calculation of the circulating composition could also be done by liquid phase density measurements with a Coriolis type sensor. However, for the given mixture the described method is favourable. The large difference in saturation temperatures of R134a and R1233zd(E) allows for a better resolution over mixture composition in comparison to the density. The mean composition of different operating points only varies marginally and thus is used to specify the reference circulating composition and thus the critical pressure. The reduced pressure for all measurements is computed in relation to the reference critical pressure. Small deviations due to a change in the circulating composition with its impact on the critical pressure are negligible.

4.1.2. State points in the test section

Knowledge of the circulating composition is not only relevant to the specification of the mixture, but also has a huge impact on the calculation of vapour quality as the state variable for partial condensation measurements. Computation by temperature and pressure measurements would assume thermodynamic equilibrium, what does not hold true for the present study. Instead, values of vapour quality

$$x = x(i, p) \tag{19}$$

are generally computed by their enthalpy and pressure dependency through REFPROP.

The mixture enters the condensation after expansion in superheated state 0 (compare Fig. 3), where

$$i_0 = i(T_0, p_0) \tag{20}$$

the enthalpy is determined by local temperature and pressure. This calculation is strongly dependent on the circulating composition. The mixture enthalpy change from point 0 to 1 is calculated as

$$i_1 = i_0(T, p) - \frac{\dot{Q}_{\mathrm{pc}}}{\dot{m}_{\mathrm{R}}}. \tag{21}$$

Here, $\dot{Q}_{\mathrm{pc}}$ is the heat flow rate transferred within the precondenser. Assuming an adiabatic system, the heat released from the mixture must be absorbed by the cooling water connected to the heat exchanger. With the water not experiencing phase change, the heat flow rate

$$\dot{Q}_{\mathrm{pc}} = \dot{m}_{\mathrm{W}} \left(i_{\mathrm{out}}(T_{\mathrm{out,W}}, p_{\mathrm{out,W}}) - i_{\mathrm{in}}(T_{\mathrm{in,W}}, p_{\mathrm{in}}) \right) \tag{22}$$

is determined by measurements of temperature, pressure and mass flow rate at the water side. Finally, the vapour quality is computed by Eq. (19). Continuing with the test section, the energy balance on the cooling water side is again used to calculate the enthalpy at the outlet (state 2). As discussed in Section 2, the cooling water energy balance is determined in a secondary cycle. The heat input of the intermediate cycle, which is connected to the test section, must be considered. Heat sources are the circulation pump and volume flow rate sensor which warms up during operation. Preliminary measurements were conducted over a wide range of operating points. The heat input $\dot{Q}_{\mathrm{imc}}$, which also represents heat losses to the ambient environment, amounts to 56 W. Similar to the calculation for the precondenser, the transferred heat flow rate

$$\dot{Q}_{\mathrm{ts}} = \dot{m}_{\mathrm{W}} \left(i_{\mathrm{out}}(T_{\mathrm{out,W}}, p_{\mathrm{out,W}}) - i_{\mathrm{in}}(T_{\mathrm{in,W}}, p_{\mathrm{in}}) \right) - \dot{Q}_{\mathrm{imc}} \tag{23}$$

and enthalpy

$$i_2 = i_1 - \frac{\dot{Q}_{\mathrm{ts}}}{\dot{m}_{\mathrm{R}}} \tag{24}$$

at state 2 are determined. The corresponding vapour quality is calculated again by Eq. (19).

4.1.3. Real and apparent heat transfer coefficients

The condensation HTC h is determined as mean value for a partial condensation with a vapour quality change of 0.05 across the test section. The general formulation of Newton's Law of Cooling

$$\dot{q} = h \left(T - T_{\mathrm{w}} \right) \tag{25}$$

states the relation between HTC and heat flux $\dot{q}$ at the heat exchanger surface with a wall temperature T_{w}. Applying Eq. (25) to the present problem, the wall temperature is defined at the inner wall of the inner tube. However, with the existing set-up, temperatures are measured at the outer wall of the inner tube. One-dimensional radial heat conduction is considered so that the inner wall temperature

$$T_{\mathrm{w,i}} = \frac{1}{16} \sum_{j=1}^{16} \left(T_{\mathrm{w,o},j} + \frac{\dot{Q}_{\mathrm{ts}} \ln\left(\frac{D_{\mathrm{w,o}}}{D_{\mathrm{w,i}}} \right)}{2\pi L k_{\mathrm{w}}} \right) \tag{26}$$

can be calculated analytically. Here, the measured wall temperature values $T_{\mathrm{w,o},a}$ correspond to the position at the outer wall of the inner tube. The fluid temperature is defined as mean value

$$T = \frac{T_1 + T_2}{2} \tag{27}$$

of the test section inlet and outlet values. The thermal conductivity of stainless steel 1.4301 k_{w} is temperature dependent and specified

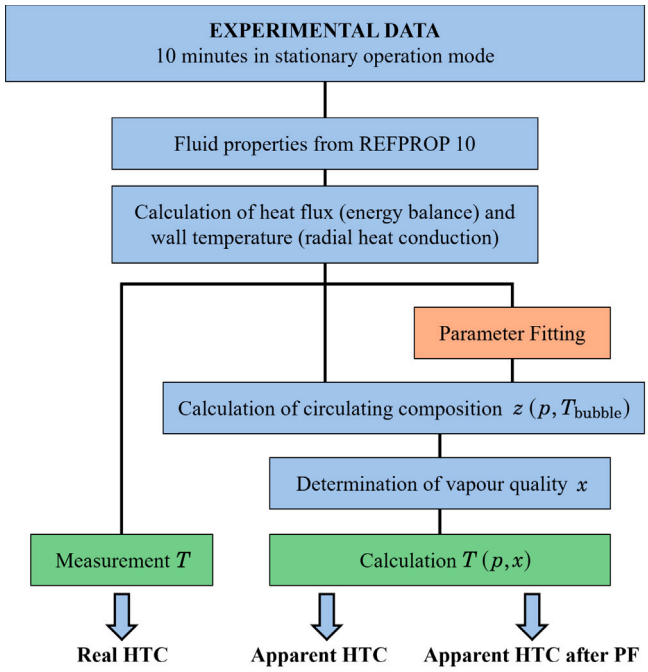

Fig. 7. Procedure of HTC determination from measurement data.

in [44]. Inserting Eqs. (26) and (27) into Eq. (25), the condensation HTC is finally calculated as

$$h = \frac{\dot{Q}_{\text{ts}}}{\pi D_{\text{w,i}} L \left[\frac{T_1+T_2}{2} - \frac{1}{16}\sum_{j=1}^{16} \left(T_{\text{w,o},j} + \frac{\dot{Q}_{\text{ts}} \ln\left(\frac{D_{\text{w,o}}}{D_{\text{w,i}}}\right)}{2\pi L k_{\text{w}}} \right) \right]}. \tag{28}$$

Commonly, the logarithmic mean temperature difference is used in heat transfer calculations rather than the difference of mean values. Resulting deviations have been investigated but are negligible due to the very low axial temperature change of the wall that is induced by the intermediate cycle. The formulation for the mixture temperature, which is given here, clearly indicates the impact of its value on the HTC calculation. As the purpose of this study is to investigate differences of the real and apparent HTC [9], two definitions for T_1 and T_2 are applied. The procedure of experimental data processing is also shown in Fig. 7. The apparent HTC, which is often reported in reference to total condensation set-ups, requires the temperature calculation

$$T_j = T(p_j, i_j) \qquad j = \{1,2\} \tag{29}$$

by pressure and enthalpy. Either default mixture properties or adapted values after parameter fitting can be used in REFPROP yielding different results. Temperature measurements are used otherwise to compute the real HTC. The sensor position in this instance has to be carefully chosen so that the temperature within the vapour bulk is recorded. A general overview of the procedure of HTC calculations from experimental data is provided in Fig. 7.

4.2. Measurement uncertainties

In order to evaluate the importance of local temperature formulation and mixture parameter fitting, the uncertainty of calculated HTCs needs to be assessed. Uncertainties of the associated influence parameters vapour quality, mass flux and reduced pressure are determined in addition to that. The methodology of uncertainty evaluation is based on the guide to the expression of uncertainties in measurement [45]. Thereby, uncertainties are categorised by types A and B. The former of these contains uncertainties that can be evaluated by statistical methods while all other sources are summarised in the latter. The type A uncertainty of any scalar output variable Y is defined as the experimental standard deviation of the mean

$$s_{\overline{Y}} = \left[\frac{1}{n-1} \sum_{j=1}^{n} \left(Y_j - \overline{Y} \right)^2 \right]^{1/2} / n^{1/2} \tag{30}$$

where the number of measurements n has a significant impact. In this study, data recording with $n = 300$ and strict requirements for stationary operation cause the type A uncertainty of calculated HTCs to be below $1\,\text{W}\,\text{m}^{-2}\,\text{K}^{-1}$.

Any given output variable Y, that is calculated depending on input variables X_a, is attributed with an uncertainty of type B by the means of uncertainties associated with all X_a. For that, Gaussian error propagation

$$u_B = \left[\sum_{j=1}^{n} \left(\frac{\partial B}{\partial A_j} \right)^2 u_{A_j}^2 + 2 \sum_{j=1}^{n-1} \sum_{l=j+1}^{n} \frac{\partial B}{\partial A_j} \frac{\partial B}{\partial A_l} u_{A_j, A_l} \right]^{1/2} \tag{31}$$

is applied to determine the standard uncertainty u_B. The second term in this equation summarises existing correlations between different input variables. This procedure of uncertainty evaluation is applied to the calculation of vapour qualities (Eq. (19)) and the HTC (Eq. (28)). An overview of the considered sensor uncertainties is given in Table 2. The specific values are representative for the default operating point ($z_{\text{R134a}} = 0.05$; $x = 0.55$; $p \ast= 0.06$; $G = 50\,\text{kg}\,\text{m}^{-2}\,\text{s}^{-1}$) but stay in the same range for other conditions.

For measurements of pressure and mass flow rate values, uncertainties by sensor specifications and the data acquisition system (DAQ) are considered. All temperature sensors were recently calibrated by a high-precision reference sensor before installation into the system. Thus, the uncertainty induced by the calibration is used in this case. It considers contributions of the reference sensor (calibration and self-heating) and the calibration environment (homogeneity and stability). An additional uncertainty in the sensor reading (resolution, self-heating and interpolation between calibrated points) is attributed. Deviations in the uncertainty between fluid and wall temperature readings mainly results from the calibration environment. All resistance temperature sensors were individually placed in an oil bath. The already installed thermocouples for wall temperature measurement were not dismantled. Instead, the test section was placed in a water bath with larger inhomogeneities for the calibration procedure. To evaluate the uncertainty of values obtained from REFPROP calculations, the central difference quotient

$$\frac{dB}{dA_j} \approx \frac{B(A_j + \Delta A_j) - B(A_j - \Delta A_j)}{2\,\Delta A_j} \qquad A_j = \{T, p, i\} \tag{32}$$

is applied for an approximation of the local derivative. The resolutions of the independent variables are $\Delta T = 1\,\text{K}$, $\Delta p = 1\,\text{kPa}$ and $\Delta i = 1\,\text{kJ}\,\text{kg}^{-1}$.

Uncertainties of geometry parameters are evaluated by tolerances originating from the manufacturing. Thereby, the uncertainties of diameters for the given condensation tube are $u_{D_{\text{w,i}}} = 0.36\,\text{mm}$ and $u_{D_{\text{w,o}}} = 0.3\,\text{mm}$. In terms of the tube length, $u_L = 2.12\,\text{mm}$. In [44], where the thermal conductivity of stainless steel 1.4301 is specified, the uncertainty is said to be $u_k = 0.035\,k$. All resulting uncertainties in this study are given as expanded measurement uncertainties U with a coverage factor of 2. The HTC uncertainty lies in the range from 5 % to 8 %, gradually increasing with the HTC. The vapour quality is determined with uncertainties in a range from 0.005 to 0.017 and the uncertainty increases at lower vapour quality values.

5. Results

5.1. Verification of results

To verify the experimental set-up and the condensation test section, measurements of the condensation heat transfer with pure R1233zd(E)

Table 2
Specification of installed sensors with their associated uncertainties in absolute numbers and relative to the reading.

Parameter	Sensor	Sources of uncertainty	Standard uncertainty	
			Absolute	Relative
Temperature refrigerant & water	Omega PR-22	Calibration, sensor reading	0.03 K	0.01 %
Temperature wall	tmg MK 93	Calibration, sensor reading	0.12 K	0.04 %
Pressure refrigerant	Omega PAA23SY	Sensor & DAQ specifications	3.6 kPa	1.59 %
Pressure water	Yokogawa FP201A	Sensor & DAQ specifications	2.1 kPa	1.85 %
Mass flow rate refrigerant	Endress + Hauser 83F15	Sensor & DAQ specifications	1.56 kg h^{-1}	1.06 %
Mass flow rate water precondenser	Endress + Hauser 83F15	Sensor & DAQ specifications	1.24 kg h^{-1}	0.93 %
Mass flow rate water cooling cycle	Bronkhorst CORI-FLOW M55	Sensor & DAQ specifications	0.46 kg h^{-1}	0.92 %

Table 3
Mean absolute percentage deviation between correlations and verification experiments conducted with pure R1233zd(E)

Shah 1979 [46]	Cavallini et al. [10]	Shah 2022 [11]	Mani Marinheiro et al. [12]
23.1	27.2	28.7	15.6

were conducted. Under variation of vapour quality, pressure and mass flux in the same range as for the mixture condensation, 45 operating points were evaluated. The resulting HTCs are in a range from 550 W m^{-2} K^{-1} to 1700 W m^{-2} K^{-1} and show a similar behaviour to that of the mixture. The HTC increases with the vapour quality and mass flux but decreases with increasing pressure. The parameter influence is discussed in detail in the following section with respect to the mixture. A comparison to four different correlations was done. Two of those – the Shah correlation from 1979 [46] and the correlation proposed by Mani Marinheiro et al. [12] – are one-equation models where no differentiation between flow regimes is made. The other correlations (Cavallini et al. [10]; Shah 2022 [11]) use different methods for calculating the condensation heat transfer coefficient depending on the flow regime. To evaluate the conducted measurements against the correlations, the mean absolute percentage deviation

$$\mathrm{MAPD} = \frac{1}{45}\sum_{1}^{45}\left|\frac{h_{\mathrm{correlation}} - h_{\mathrm{experiment}}}{h_{\mathrm{experiment}}}\right| \tag{33}$$

was calculated. The corresponding values are given in Table 3. The numerical HTC and correlation results are additionally listed in the appendix. The correlations are reported with MAPDs ranging from 14 % to 23.3 % to their considered data bases and thus the obtained results verify the condensation test section.

5.2. Condensation heat transfer coefficients

Condensation HTCs were determined as real and apparent values for two different compositions of the mixture R134a/R1233zd(E). The calculation was also performed using sensor data from the intermediate cooling cycle, but yields measurement uncertainties for the HTC of approximately 80 %. Therefore, a possible comparison of this direct cooling evaluation with the thermal amplification technique, which was generally applied in this study, would require further trade-offs in the condensation heat duty beyond this study.

The experimental data exhibits HTCs in the range between 500 W m^{-2} K^{-1} to 1100 W m^{-2} K^{-1} and is discussed depending on the chosen influence parameters. The highest sensitivity is attributed to the change of vapour quality as shown in Fig. 8. The HTC increases almost linearly with x with large relative changes due to the generally low values. The slope is comparable to data from Cavallini et al. [47] for R134a, where the difference between the maximal and minimal HTC values was about 500 W m^{-2} K^{-1} at the lowest investigated mass flux. The authors stated that these characteristic moderate increases of HTCs in stratified flow indicate the vapour shear force to be negligible at low mass fluxes. In annular condensation flow, a steeper increase with the vapour quality was found. This phenomenon is due to the liquid film thickness strongly depending on the vapour quality, whereas

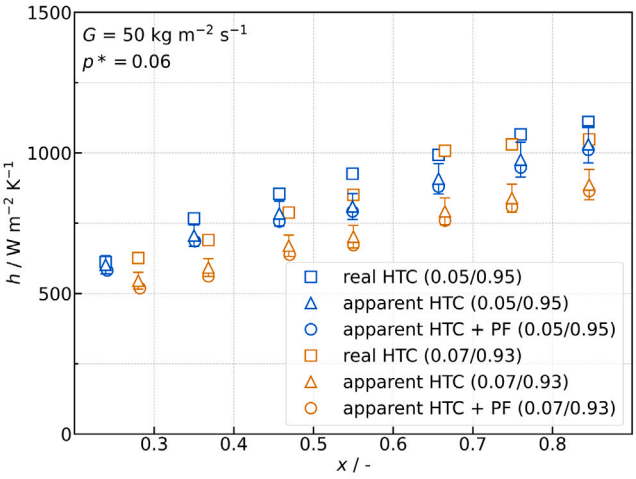

Fig. 8. Experimentally determined HTCs depending on vapour quality.

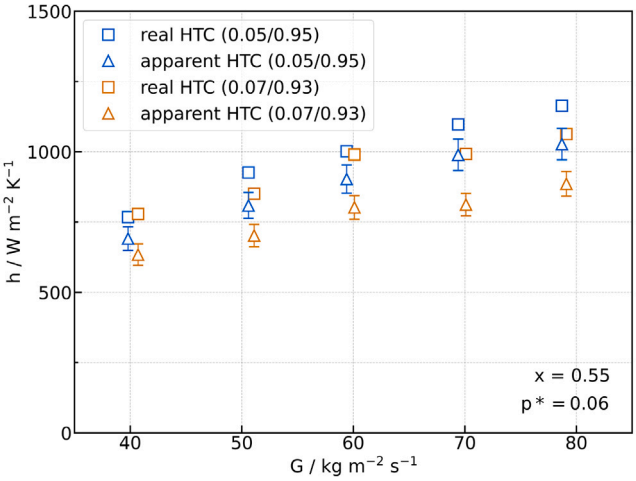

Fig. 9. Experimentally determined HTCs depending on mass flux.

condensation in stratified flow always occurs in proximity of the tube wall and mainly the changing void fraction influences the HTC by the proportions of film condensation and single-phase convective heat transfer. The dependency on mass flux, which is depicted in Fig. 9, is linked to effects of the flow velocity. Higher velocities cause increased fluid mixing, a reduction in the mass transfer resistance at the condensation interface and thus better convective heat transfer.

Finally, the HTC also exhibits sensitivity to pressure as shown in Fig. 10. In contrast to vapour quality and mass flux, values increase at lower pressures. The data indicates that especially at low pressures a larger increase of HTCs can be achieved by changes in

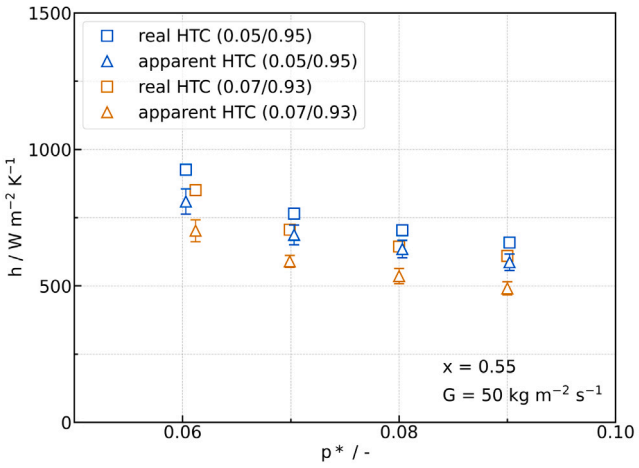

Fig. 10. Experimentally determined HTCs depending on reduced pressure.

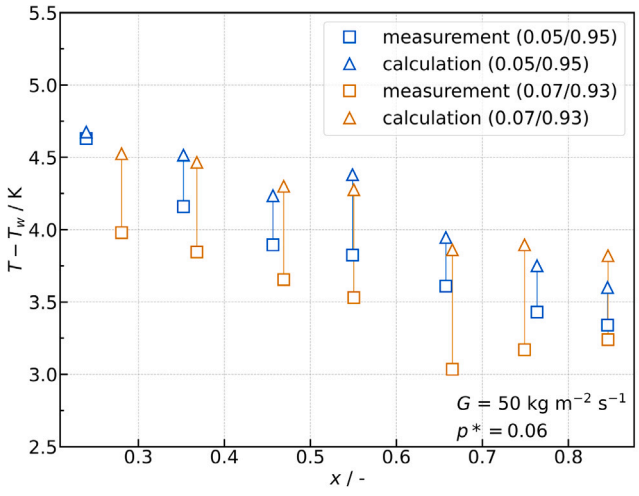

Fig. 11. Comparison of measured and calculated local fluid temperatures in difference to wall temperature.

the condensation pressure. The pressure influence is related to the temperature-dependent properties density, viscosity and thermal conductivity. Thus, the variation of HTCs with pressure is specific to a distinct fluid.

A difference in the HTC between real and apparent value is given across all operating conditions where the former of these is always higher than the latter. In relative numbers, the deviation ranges from 8 % to 12 % for the majority of measurements at $z_{R134a} = 0.05$ and from 13 % to 20 % at $z_{R134a} = 0.07$. Only at low vapour qualities, real and apparent HTCs converge. As per definition of the HTC, the differentiation originates solely from the fluid temperature formulation. The temperature difference $\Delta T = T - T_w$ is depicted in Fig. 11 for the measurements with varying vapour quality. Outlying points in this representation ($x = 0.65$ and $x = 0.75$ at $z_{R134a} = 0.07$) are caused by smaller variations of vapour quality in the test section and do not imply outliers in the HTC as can be seen in Fig. 8.

A comparison between measured and calculated temperatures can only be drawn for individual measurements due to variations in the heat flow rate. Calculated temperatures are generally higher than measured values, and the difference increases with the mass fraction of R134a. As a consequence, temperature measurement of superheated vapour does not take place. Subcooling of liquid phase on the other hand is as well no explanation due to the verified positioning of sensors in the vapour phase. Systematic errors in the fluid temperature measurements, which could explain the continuous behaviour of lower values, can be excluded. In preliminary tests with pure R1233zd(E), the discrepancy was generally lower than 0.1 K. One possible source for the deviations lies in the approximated mixture properties. Wrong prediction of the VLE data would cause a difference in the temperature calculation. The key role, however, is assumedly taken by local composition shift in the test section. The condensation process is taking place in proximity of the tube wall, and no liquid film formation can be observed due to the dominant gravity force at low mass fluxes. Due to the fractionation potential of the mixture, the condensate is enriched in the less volatile component R1233zd(E). This leads to higher mass fraction of R134a in the vapour phase close to the tube wall in comparison to the vapour bulk. A similar phenomenon was measured and reported by Zhang et al. [48] in stratified flow of a mixture R134a/R245fa. While the authors used a different geometry in form of a rectangular channel, the were able to measure the local composition of the vapour phase at different heights. Significant differences in the concentration of R134a were determined between the lower and upper sampling point. Translating their findings to the present work, a radial composition shift appears to be the plausible reason for temperature gradients in the vapour phase of the two-phase flow. This explains deviations between measurement and calculation but also provides reasoning for the outlier in Fig. 11 at the lowest measured vapour quality. The temperature glide of the mixture R134a/R1233zd(E) is not linear over the vapour quality but has a steep increase at low x values. This highlights the large difference between vapour and liquid phase composition of the mixture, causing the vapour phase at low vapour qualities to mainly consist of R134a. Consequently, the reported composition gradient diminishes in this instance causing the measured and calculated temperatures to be similar. The results still show the need of a more comparable temperature measurement position in experimental studies.

5.3. Influence of mixture parameter fitting

The circulating composition is determined by the bubble point within the evaporator. Pressure and temperature are measured, where the temperature value is assumed to represent the local bubble point temperature at the given pressure. The change in composition, which results from parameter fitting explained in Section 3 is about 0.2 % across all operating points, and can be seen in Fig. 12 exemplarily for the default case. The histogram shows the distribution of the concentration of R1233zd(E) where more than 90 % of values are within a range of 0.001 – which is also the digit where rounding takes place.

The visible uncertainty in the concentration indicates the impact of the parameter fitting. The former concentration, calculated before parameter fitting using estimated parameters and depicted by a red line, is outside of any reasonable credible interval of the samples. Thus, given the predicted VLE data with their uncertainties from GEMC simulations, the updated interaction parameters should be used for further property calculations. Contrarily, the impact of parameter fitting on the vapour quality calculation is negligible. The mean of the distribution after parameter fitting is identical to the a priori calculated vapour quality. Due to rounding the values of vapour quality to the third decimal, minimal changes are overwritten. In addition to that, the effect of uncertainties in the HEOS is outweighed as the difference between minimum and maximum vapour quality is less than 0.001. A minor change in the calculated vapour quality after parameter fitting exists only at low vapour qualities.

The final evaluation of parameter fitting against the determined HTCs yields a visible influence which is, however, smaller than the impact of temperature definition in the differentiation between real and

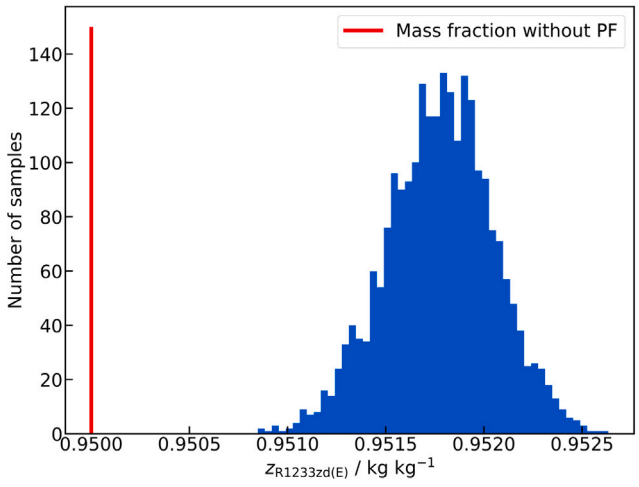

Fig. 12. Histogram showing the mass fraction of R1233zd(E) after parameter fitting with $n = 2400$ samples.

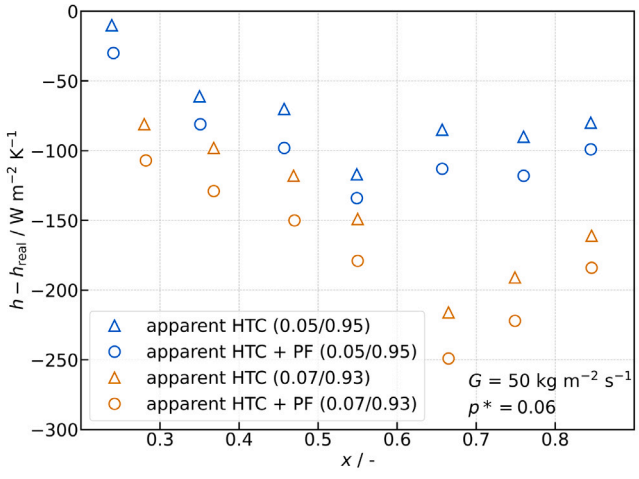

Fig. 13. Deviation between real and apparent HTCs before and after parameter fitting.

apparent HTC. As depicted in Fig. 8, the difference between results without and with parameter fitting is in the range of measurement uncertainties for all operating conditions. It has to be noted that parameter fitting increases the deviation from real HTC values, which is shown again for the identical data in Fig. 13. The depiction reveals the trend of underestimated apparent HTCs, also being influenced by the vapour quality. The deviation between values before and after parameter fitting, on the other hand, is about constant. It remains in the range of 20 W m^{-2} K^{-1} to 30 W m^{-2} K^{-1}. At this point, the effect of composition change due to parameter fitting comes to play. The shift to larger mass fractions of R1233zd(E) consequences an increase of dew and bubble point temperature for the circulating mixture. This also causes higher local fluid temperatures in the condenser, even though the vapour quality does not change with parameter fitting. The calculation of higher fluid temperatures finally causes lower HTCs. Thus, the obtained measurement results indicate that the largest impact of parameter fitting is on the VLE data at lower pressures due to a different composition in the cycle.

6. Conclusion and outlook

The present study investigated uncertainties in the experimental determination of HTCs for film condensation of the zeotropic mixture R134a/R1233zd(E) in a horizontal tube. The results indicate that peculiarities in the systematics can outweigh measurement uncertainties obtained from evaluation of sensor and data processing equipment. An ORC test rig was used to determine HTCs in stationary operating mode for varying vapour quality, mass flux and pressure. Three different aspects reported in literature were considered regarding their influence on HTCs:

- In stratified flow condensation of zeotropic mixtures, the assumption of thermodynamic equilibrium does not fully hold true. Local temperature deviations between the phases in a liquid-vapour mixture effect the HTC values depending on the fluid temperature definition. The real HTC – defined by the measurement of the vapour phase temperature – was found to be higher than the apparent value which considers the calculated local dew point temperature $T_{dew}(z, p)$ under all investigated operating conditions.
- The effect of fitting interaction parameters to GEMC simulation data in order to achieve high-fidelity mixture properties was evaluated as such data had not been published before. The resulting interaction parameter means showed a suitable fit to the GEMC data. However, the predicted uncertainty intervals did not fully cover the data, hence the parameter uncertainty is probably underestimated. The remaining error could for example be attributed to model error. The difference in VLE calculations after parameter fitting was apparent in the results in terms of a consistent change in the circulating composition which was derived from the bubble point temperature. The resulting HTCs were lower after parameter fitting with the deviation being almost constant and in the range of measurement uncertainties.
- A complete evaluation of the used thermal amplification technique was not done due to the measurement uncertainties of the HTCs reaching values of 80 %. It is apparent that only the thermal amplification technique allows to conduct measurements during a partial condensation with a low variation of the vapour quality and averaging of results. In order to compare measurements with and without the technique, an adapted study design with higher heat flow rates in the test section would be needed.

Expanded uncertainties for the HTCs were reported in a range between 5 % to 8 %. The impact of fluid temperature definition was found to outweigh them under almost all operating conditions. The change of HTCs after parameter fitting increased the deviation between real and apparent value while not being that significant. Future research should, however, consider further uncertainties in the parameter fitting, if available VLE data does not overlap with the given operating range. This was not investigated in the present work where the GEMC simulations were purposely done for the required pressure range. This study concludes that the experimental determination of HTCs for zeotropic mixtures is subject to higher uncertainties than for pure fluids due to the analysed aspects. The key findings of this study may be transferred to any zeotropic mixture. The deviation between real and apparent HTC is assumedly dependent on the temperature glide and thus the specific mixture. They could be outweighed by the effect of parameter fitting for newly applied mixtures. This is especially relevant due to the environmental impact of refrigerants that is nowadays a key factor in energy technology development. Therefore, the assumption of thermodynamic equilibrium and the availability of mixture properties should be taken into consideration in future research.

Table A.1
GEMC simulation results and their standard deviations for the compositions $X^{(bubble)}$, $X^{(dew)}$ and saturated densities $\varrho^{(bubble)}$, $\varrho^{(dew)}$ of R134a/R1233zd(E).

T/K	p/MPa	$X^{(bubble)}_{R134a}$/mol mol^{-1}	$X^{(dew)}_{R134a}$/mol mol^{-1}	$\rho^{(bubble)}$/kg m^{-3}	$\rho^{(dew)}$/kg m^{-3}
293.15	0.15	0.066 (0.005)	0.294 (0.012)	1278.4 (3.2)	7.88 (0.02)
293.15	0.20	0.161 (0.006)	0.507 (0.024)	1273.3 (2.0)	10.06 (0.07)
293.15	0.25	0.255 (0.017)	0.641 (0.020)	1270.1 (3.0)	12.26 (0.06)
293.15	0.30	0.352 (0.015)	0.734 (0.013)	1265.0 (2.8)	14.50 (0.07)
293.15	0.40	0.565 (0.023)	0.860 (0.013)	1251.4 (3.0)	19.06 (0.06)
293.15	0.50	0.786 (0.005)	0.940 (0.002)	1234.1 (2.1)	23.76 (0.08)
333.15	0.50	0.056 (0.003)	0.185 (0.008)	1168.0 (5.4)	25.13 (0.74)
333.15	0.60	0.139 (0.008)	0.380 (0.018)	1160.2 (2.2)	29.34 (0.14)
333.15	0.70	0.210 (0.013)	0.489 (0.021)	1153.7 (2.4)	33.70 (0.30)
333.15	0.80	0.277 (0.023)	0.574 (0.030)	1150.8 (6.1)	38.41 (0.32)
333.15	1.00	0.423 (0.018)	0.706 (0.016)	1137.7 (5.7)	47.68 (0.41)
333.15	1.20	0.589 (0.017)	0.816 (0.009)	1114.7 (4.6)	57.21 (0.34)

CRediT authorship contribution statement

Clemens Berger: Writing – review & editing, Writing – original draft, Visualization, Validation, Methodology, Investigation, Formal analysis, Data curation, Conceptualization. **Leonard Schnelting:** Writing – review & editing, Writing – original draft, Visualization, Methodology, Investigation, Formal analysis, Conceptualization. **Gabriele Raabe:** Writing – review & editing, Writing – original draft, Supervision, Project administration, Methodology, Investigation, Funding acquisition, Formal analysis, Conceptualization. **Matthias Welzl:** Writing – review & editing, Supervision, Resources, Methodology, Funding acquisition, Conceptualization. **Florian Heberle:** Writing – review & editing, Visualization, Supervision, Project administration, Methodology, Funding acquisition, Conceptualization. **Dieter Brüggemann:** Writing – review & editing, Supervision, Project administration, Funding acquisition.

Declaration of Generative AI and AI-assisted technologies in the writing process

During the preparation of this work, the authors used GitHub Copilot. The authors reviewed and checked every line of code and take full responsibility for the content of the publication.

Declaration of competing interest

The authors declare that they have no known competing financial interests or personal relationships that could have appeared to influence the work reported in this paper.

Acknowledgements

The authors thank Ulrich Römer (Institute for Acoustics and Dynamics, Technische Universität Braunschweig) for his methodological input and his support in review and editing.

This work was funded by the Deutsche Forschungsgemeinschaft (DFG, German Research Foundation), Germany as part of the Priority Programme – SPP 2403 "Carnot Batteries: Inverse Design from Markets to
Molecules" – 526234111; 526254705. Further funding was provided by DFG- INST 91/437-1 FUGG. The authors gratefully acknowledge all funding sources.

Appendix A. Gibbs ensemble Monte Carlo simulations for the zeotropic mixture R134a/R1233zd(E)

Predictions for the VLE of the zeotropic mixture R134a/R1233zd(E) were derived by GEMC simulations [49] in the isothermal–isobaric (NPT) ensemble using the simulation code TOWHEE [50]. The refrigerant R134a was modelled by the all-atoms force field by Peguin et al. [51], whereas the transferable H(C)FO model developed in the Raabe group [52] was employed to model the HCFO R1233zd(E). The Lennard Jones parameters for interactions between unlike atoms were obtained from the Lorentz–Berthelot combining rule with no adjustable interaction parameters, resulting in purely predictive VLE data for the mixtures. Each system consisted of 432 molecules in total, but depending on the state point, the number of the molecules of both components were varied to yield a feed composition within the two phase region. Electrostatic interactions were treated via the Ewald summation method [53] using a cut-off radius equal to half the box length, while a 12 Å cut-off was applied to the Lennard–Jones interactions. Standard long-range corrections were applied to both the energy and the pressure (see for instance [39]). For each data point, the simulation was equilibrated for 120000 to 200000 cycles. The production runs comprised 400000 cycles from which ensemble averages for the compositions and saturated densities of the coexisting phases at the specified temperature and pressure were obtained. Standard deviations of the ensemble averages for the compositions and densities were determined by the standard block averaging technique (e.g. [39]). The GEMC simulation results for the compositions and the saturated densities of the liquid and vapour phase of the VLE in the zeotropic mixture R134a/R1233zd(E) at $T = 293.15$ K and 333.15 K are summarised in the following Table A.1.

Appendix B. Experimental heat transfer results of verification measurements

The results in Table B.2 were obtained in verification measurements for condensation of pure R1233zd(E). The reported HTC values apply the measured saturation temperature and are thus comparable to the real HTCs for the mixture.

Data availability

Data will be made available on request.

Table B.2
Experimental heat transfer coefficients and correlation results of verification measurements with pure R1233zd(E).

p/kPa	G/kg m^{-2} s^{-1}	x/-	h/W m^{-2} K^{-1}	Shah 1979	Cavallini et al.	Shah 2022	Mani Marinheiro et al.
181.0	39.6	0.266	1013	451	439	877	670
181.0	39.3	0.415	1153	586	567	1047	852
181.5	39.4	0.559	1258	702	689	1209	990
180.8	39.2	0.709	1340	802	813	1386	1088
181.0	39.2	0.858	1341	882	938	1622	1137
181.2	59.5	0.303	1240	676	601	1059	902
181.0	59.4	0.412	1370	810	733	1217	1064
180.9	59.2	0.562	1459	975	911	1427	1242
180.8	59.3	0.714	1550	1122	1092	1641	1369
181.1	59.8	0.849	1569	1233	1262	1871	1433
181.1	77.1	0.243	1204	730	624	1074	920
181.5	77.8	0.418	1367	1014	896	1393	1244
181.1	78.6	0.547	1533	1202	1103	1614	1432
181.2	79.1	0.684	1630	1377	1321	1841	1579
181.0	79.2	0.849	1704	1542	1580	2132	1672
217.9	40.0	0.257	690	426	389	843	637
217.4	38.9	0.407	792	546	517	1001	806
218.3	40.0	0.561	941	674	631	1174	959
217.1	40.3	0.695	1032	768	741	1332	1053
217.6	40.0	0.826	1079	835	840	1515	1099
216.4	60.1	0.243	917	572	490	938	774
217.4	59.5	0.395	992	754	653	1151	1002
217.4	59.9	0.547	1079	919	826	1358	1185
217.2	60.0	0.702	1157	1062	999	1567	1315
217.4	60.1	0.842	1196	1166	1157	1787	1379
217.4	78.0	0.239	1022	698	587	1036	884
217.3	78.3	0.423	1175	977	851	1351	1208
217.1	78.5	0.547	1213	1141	1022	1548	1375
217.0	78.3	0.717	1191	1331	1258	1807	1534
216.9	78.2	0.841	1243	1440	1432	2015	1595
253.8	39.9	0.267	560	418	386	833	628
253.7	38.9	0.401	729	519	481	967	772
253.7	40.6	0.544	792	643	596	1129	922
254.2	38.5	0.698	811	710	679	1276	993
253.6	39.1	0.846	890	791	797	1496	1052
253.5	60.6	0.264	729	581	493	946	787
253.5	60.5	0.414	866	753	650	1149	1001
253.2	60.5	0.549	941	889	791	1323	1153
253.5	60.2	0.714	1003	1028	957	1533	1280
253.5	61.3	0.854	1032	1137	1119	1763	1349
254.0	78.9	0.258	895	708	583	1044	898
253.2	78.7	0.414	985	930	787	1297	1158
253.3	78.7	0.555	1042	1104	971	1508	1338
253.5	78.3	0.701	1062	1256	1155	1718	1470
253.3	78.7	0.854	1135	1390	1363	1973	1549

References

[1] R. Jakobs, H. Kruse, The use of non-azeotropic refrigerant mixtures in heat pumps for energy saving, Int. J. Refrig. 2 (1) (1979) 29–32, http://dx.doi.org/10.1016/0140-7007(79)90101-4.

[2] H. Kruse, The advantages non-azeotropic refrigerant mixtures for heat pump application, Int. J. Refrig. 4 (3) (1981) 119–125, http://dx.doi.org/10.1016/0140-7007(81)90102-X.

[3] W.F. Stoecker, D. Walukas, Conserving energy in domestic refrigerators through the use of refrigerant mixtures, Int. J. Refrig. 4 (4) (1981) 201–208, http://dx.doi.org/10.1016/0140-7007(81)90051-7.

[4] C.J. Bliem, Zeotropic mixtures of halocarbons as working fluids in binary geothermal power generation cycles, in: 22nd Intersociety Energy Conversion Engineering Conference, American Institute of Aeronautics and Astronautics, Reston, Virginia, 1987, pp. 930–935, http://dx.doi.org/10.2514/6.1987-9380.

[5] D.A. Didion, D.B. Bivens, Role of refrigerant mixtures as alternatives to CFCs, Int. J. Refrig. 13 (3) (1990) 163–175, http://dx.doi.org/10.1016/0140-7007(90)90071-4.

[6] Q. Chen, J. Yu, G. Yan, Performance analysis of a modified zeotropic mixture (R290/R600) refrigeration cycle with internal subcooler for freezer applications, Appl. Therm. Eng. 108 (2016) 172–180, http://dx.doi.org/10.1016/j.applthermaleng.2016.07.132.

[7] Y. Huang, J. Chen, Y. Chen, X. Luo, Y. Liang, J. He, Z. Yang, Performance explorations of a novel high temperature heat pump with multi-adjusted compositions of zeotropic mixture, Appl. Therm. Eng. 235 (2023) 121409, http://dx.doi.org/10.1016/j.applthermaleng.2023.121409.

[8] F. Heberle, M. Preißinger, D. Brüggemann, Zeotropic mixtures as working fluids in Organic Rankine Cycles for low-enthalpy geothermal resources, Renew. Energy 37 (1) (2012) 364–370, http://dx.doi.org/10.1016/j.renene.2011.06.044.

[9] B.M. Fronk, S. Garimella, In-tube condensation of zeotropic fluid mixtures: A review, Int. J. Refrig. 36 (2) (2013) 534–561, http://dx.doi.org/10.1016/j.ijrefrig.2012.11.030.

[10] A. Cavallini, D. Del Col, L. Doretti, M. Matkovic, L. Rossetto, C. Zilio, G. Censi, Condensation in horizontal smooth tubes: A new heat transfer model for heat exchanger design, Heat Transf. Eng. 27 (8) (2006) 31–38, http://dx.doi.org/10.1080/01457630600793970.

[11] M.M. Shah, Improved correlation for heat transfer during condensation in mini and macro channels, Int. J. Heat Mass Transfer 194 (2022) 123069, http://dx.doi.org/10.1016/j.ijheatmasstransfer.2022.123069.

[12] M. Mani Marinheiro, D. Borba Marchetto, G. Furlan, A. Theodoro de Souza Netto, C. Bigonha Tibiriçá, A robust and simple correlation for internal flow condensation, Appl. Therm. Eng. 236 (2024) 121811, http://dx.doi.org/10.1016/j.applthermaleng.2023.121811.

[13] D.B. Marchetto, M.M. Marinheiro, A.T. de Souza Netto, G. Furlan, G. Ribatski, J.R. Thome, C.B. Tibiriçá, Condensation flow inside tubes: A review of heat transfer coefficient measurement techniques, experimental databases and prediction methods, Exp. Therm. Fluid Sci. 160 (2025) 111298, http://dx.doi.org/10.1016/j.expthermflusci.2024.111298.

[14] T.A. Jacob, B.M. Fronk, Experimental investigation of low GWP alternative R1233zd(E) for use in organic rankine cycle condensers, in: IIR Rankine International Conference, 2020, pp. 108–115, http://dx.doi.org/10.18462/iir.rankine.2020.1122.

[15] M. Azzolin, S. Bortolin, D. Del Col, Convective condensation at low mass flux: Effect of turbulence and tube orientation on the heat transfer, Int. J. Heat Mass Transfer 144 (2019) 118646, http://dx.doi.org/10.1016/j.ijheatmasstransfer.2019.118646.

[16] S. Mazumder, H. Afroz, M.A. Hossain, A. Miyara, S. Talukdar, Study of in-tube condensation heat transfer of zeotropic R32/R1234ze(E) mixture refrigerants,

Int. J. Heat Mass Transfer 169 (2021) 120859, http://dx.doi.org/10.1016/j.ijheatmasstransfer.2020.120859.
[17] L. Wang, P. Jiao, C. Dang, E. Hihara, B. Dai, Condensation heat and mass transfer characteristics of low GWP zeotropic refrigerant mixture R1234yf/R32 inside a horizontal smooth tube: An experimental study and non-equilibrium film model development, Int. J. Therm. Sci. 170 (2021) 107090, http://dx.doi.org/10.1016/j.ijthermalsci.2021.107090.
[18] H.-S. Lee, C.-H. Son, Condensation heat transfer and pressure drop characteristics of R-290, R-600a, R-134a and R-22 in horizontal tubes, Heat Mass Transf. 46 (5) (2010) 571–584, http://dx.doi.org/10.1007/s00231-010-0603-9.
[19] T.A. Moreira, Z.H. Ayub, G. Ribatski, Convective condensation of R600a, R290, R1270 and their zeotropic binary mixtures in horizontal tubes, Int. J. Refrig. 130 (2021) 27–43, http://dx.doi.org/10.1016/j.ijrefrig.2021.06.031.
[20] M.K. Dobson, J.C. Chato, J.P. Wattelet, J.A. Gaibel, M. Ponchner, P.J. Kenney, R.L. Shimon, T.C. Villaneuva, N.L. Rhines, K.A. Sweeney, D.G. Allen, T.T. Hershberger, Heat transfer and flow regimes during condensation in horizontal tubes, Air Cond. Refrig. Cent. Tech. Rep. 57 (1) (1994).
[21] W. Li, W. Tang, J. Chen, H. Zhu, D.J. Kukulka, Y. He, Z. Sun, J. Du, B. Zhang, Convective condensation in three enhanced tubes with different surface modifications, Exp. Therm. Fluid Sci. 97 (2018) 79–88, http://dx.doi.org/10.1016/j.expthermflusci.2018.04.011.
[22] H. Nasrfard, H. Rahimzadeh, A. Ahmadpour, H. Naderan, Experimental study of condensation heat transfer for R141b in intermittent flow regime within a smooth horizontal tube, Exp. Therm. Fluid Sci. 105 (2019) 109–122, http://dx.doi.org/10.1016/j.expthermflusci.2019.03.019.
[23] J.P. Meyer, D. Ewim, Heat transfer coefficients during the condensation of low mass fluxes in smooth horizontal tubes, Int. J. Multiph. Flow 99 (2018) 485–499, http://dx.doi.org/10.1016/j.ijmultiphaseflow.2017.11.015.
[24] A.O. Adelaja, D.R. Ewim, J. Dirker, J.P. Meyer, Heat transfer, void fraction and pressure drop during condensation inside inclined smooth and microfin tubes, Exp. Therm. Fluid Sci. 109 (2019) 109905, http://dx.doi.org/10.1016/j.expthermflusci.2019.109905.
[25] H. Deng, M. Rossato, M. Fernandino, D. Del Col, A new simplified model for condensation heat transfer of zeotropic mixtures inside horizontal tubes, Appl. Therm. Eng. 153 (2019) 779–790, http://dx.doi.org/10.1016/j.applthermaleng.2019.02.128.
[26] S. Garimella, T.M. Bandhauer (Eds.), Measurement of condensation heat transfer coefficients in microchannel tubes, in: ASME International Mechanical Engineering Congress and Exposition, in: Fluid-Physics and Heat Transfer for Macro- and Micro-Scale Gas-Liquid and Phase-Change Flows, vol. 3, 2001, http://dx.doi.org/10.1115/IMECE2001/HTD-24221.
[27] T.M. Bandhauer, A. Agarwal, S. Garimella, Measurement and modeling of condensation heat transfer coefficients in circular microchannels, J. Heat Transf. 128 (10) (2006) 1050–1059, http://dx.doi.org/10.1115/1.2345427.
[28] G. Ghim, J. Lee, Experimental evaluation of the in-tube condensation heat transfer of pure n -pentane/R245fa and their non-azeotropic mixture as an ORC working fluid, Appl. Therm. Eng. 106 (2016) 753–761, http://dx.doi.org/10.1016/j.applthermaleng.2016.06.023.
[29] G. Ghim, J. Lee, Condensation heat transfer of low GWP ORC working fluids in a horizontal smooth tube, Int. J. Heat Mass Transfer 104 (2017) 718–728, http://dx.doi.org/10.1016/j.ijheatmasstransfer.2016.08.090.
[30] B.M. Fronk, S. Garimella, Condensation of ammonia and high-temperature-glide ammonia/water zeotropic mixtures in minichannels – Part I: Measurements, Int. J. Heat Mass Transfer 101 (2016) 1343–1356, http://dx.doi.org/10.1016/j.ijheatmasstransfer.2016.05.049.
[31] E.W. Lemmon, I.H. Bell, M.L. Huber, M.O. McLinden, NIST standard reference database 23: Reference fluid thermodynamic and transport properties-REFPROP, Version 10.0, National Institute of Standards and Technology, 2018, http://dx.doi.org/10.18434/T4/1502528, URL https://www.nist.gov/srd/refprop.
[32] M. Welzl, F. Heberle, D. Brüggemann, Influence of wall material on heat transfer in nucleate pool boiling of refrigerants, in: Proceeding of International Heat Transfer Conference 17, Begellhouse, Connecticut, 2023, p. 11, http://dx.doi.org/10.1615/IHTC17.360-60.
[33] M. Welzl, Untersuchung des Wärmeübergangs und der Leistungsabgabe bei Einsatz von Arbeitsmedien mit geringem Treibhauspotenzial im Organic Rankine Cycle: Dissertation, in: Thermodynamik, vol. 41, Logos, Berlin, 2023 (in German).
[34] F. Heberle, Untersuchungen zum Einsatz von zeotropen Fluidgemischen im Organic Rankine Cycle für die geothermische Stromerzeugung: Dissertation, in: Thermodynamik, vol. 22, Logos, Berlin, 2013 (in German).
[35] European Union, Regulation (EU) 2024/573 of the European Parliament and of the Council of 7 February 2024 on fluorinated greenhouse gases, amending Directive (EU) 2019/1937 and repealing Regulation (EU) No 517/2014, Off. J. Eur. Union 2024/573 (L 2024/573) (2024).
[36] J. Chen, H. Kruse, Calculating circulation concentration of zeotropic refrigerant mixtures, HVAC&R Res. 1 (3) (1995) 219–231, http://dx.doi.org/10.1080/10789669.1995.10391320.
[37] E.W. Lemmon, R. Tillner-Roth, A Helmholtz energy equation of state for calculating the thermodynamic properties of fluid mixtures, Fluid Phase Equilib. 165 (1) (1999) 1–21, http://dx.doi.org/10.1016/S0378-3812(99)00262-9.
[38] O. Kunz, W. Wagner, The GERG-2008 wide-range equation of state for natural gases and other mixtures: An expansion of GERG-2004, J. Chem. Eng. Data 57 (11) (2012) 3032–3091, http://dx.doi.org/10.1021/je300655b.
[39] G. Raabe, Molecular Simulation Studies on Thermophysical Properties, Springer, Singapore, 2017, http://dx.doi.org/10.1007/978-981-10-3545-6.
[40] L. Schnelting, B.G. Bederna, G. Raabe, U. Römer, C. Thomas, Bayesian calibration of HEOS mixing models and impact on thermodynamic cycles, in: The 38th International Conference on Efficiency, Cost, Optimization, Simulation and Environmental Impact of Energy Systems, 2025, http://dx.doi.org/10.26434/chemrxiv-2025-vnm16.
[41] I.H. Bell, E.W. Lemmon, Automatic fitting of binary interaction parameters for multi-fluid Helmholtz-energy-explicit mixture models, J. Chem. Eng. Data 61 (11) (2016) 3752–3760, http://dx.doi.org/10.1021/acs.jced.6b00257.
[42] J. Goodman, J. Weare, Ensemble samplers with affine invariance, Commun. Appl. Math. Comput. Sci. 5 (1) (2010) 65–80, http://dx.doi.org/10.2140/camcos.2010.5.65.
[43] D. Foreman-Mackey, D.W. Hogg, D. Lang, J. Goodman, emcee : The MCMC hammer, Publ. Astron. Soc. Pac. 125 (925) (2013) 306–312, http://dx.doi.org/10.1086/670067.
[44] P. Stephan, S. Kabelac, M. Kind, D. Mewes, K. Schaber, T. Wetzel, VDI-Wärmeatlas, 12. Auflage, in: VDI Springer Reference, Springer Vieweg, VDI-Gesellschaft Verfahrenstechnik und Chemieingenieurwesen and Springer-Verlag GmbH, Berlin and Heidelberg, 2019, http://dx.doi.org/10.1007/978-3-662-52989-8, (in German).
[45] Joint Committee for Guides in Metrology, Evaluation of measurement data — Guide to the expression of uncertainty in measurement, Joint Committee for Guides in Metrology, 2008, http://dx.doi.org/10.59161/JCGM100-2008E.
[46] M.M. Shah, A general correlation for heat transfer during film condensation inside pipes, Int. J. Heat Mass Transfer 22 (4) (1979) 547–556, http://dx.doi.org/10.1016/0017-9310(79)90058-9.
[47] A. Cavallini, D. Del Col, L. Doretti, L. Rossetto, G.A. Longo, Condensation heat transfer of new refrigerants: Advantages of high pressure fluids, in: International Refrigeration and Air Conditioning Conference, 2000, paper number 480.
[48] Y. Zhang, L. Jia, C. Dang, Z. Qi, The mass transfer characteristics of R134a/R245fa during stratified flow condensation in rectangular channel, Int. J. Heat Mass Transfer 195 (2022) 123189, http://dx.doi.org/10.1016/j.ijheatmasstransfer.2022.123189.
[49] A.Z. Panagiotopoulos, Direct determination of phase coexistence properties of fluids by Monte Carlo simulation in a new ensemble, Mol. Phys. 61 (4) (1987) 813–826, http://dx.doi.org/10.1080/00268978700101491.
[50] M.G. Martin, MCCCS towhee: a tool for Monte Carlo molecular simulation, Mol. Simul. 39 (14–15) (2013) 1212–1222, http://dx.doi.org/10.1080/08927022.2013.828208.
[51] R.P.S. Peguin, G. Kamath, J.J. Potoff, S.R.P. Da Rocha, All-atom force field for the prediction of vapor-liquid equilibria and interfacial properties of HFA134a, J. Phys. Chem. B 113 (1) (2009) 178–187, http://dx.doi.org/10.1021/jp806213w.
[52] G. Raabe, Parameterization approach for a systematic extension of the hydrofluoroolefin force field to fluorinated butenes and hydrochlorofluoroolefin compounds, J. Chem. Eng. Data 65 (3) (2020) 1234–1242, http://dx.doi.org/10.1021/acs.jced.9b00588.
[53] P.P. Ewald, Die Berechnung optischer und elektrostatischer Gitterpotentiale, Ann. Phys., Lpz. 369 (3) (1921) 253–287, http://dx.doi.org/10.1002/andp.19213690304 (in German).